

# Microfluidic *In Situ* Measurement of Poisson's Ratios of Hydrogels

Jean Cappello<sup>1</sup>, Vincent d'Herbement<sup>1</sup>, Anke Lindner<sup>1,\*</sup> and Olivia du Roure<sup>1</sup>  
<sup>1</sup> Laboratoire PMMH-ESPCI Paris, PSL Research University,  
Sorbonne Université, Université de Paris, 10, rue Vauquelin, Paris, France

Being able to precisely characterize the mechanical properties of soft microparticles is essential for numerous situations from the understanding of the flow of biological fluids to the development of soft micro-robots. Here we present a simple measurement technique for the Poisson's ratio of soft micron-sized hydrogels in the presence of a surrounding liquid. This method relies on the measurement of the deformation in two orthogonal directions of a rectangular hydrogel slab compressed uni-axially inside a microfluidic channel. Due to the *in situ* character of the method, the sample does not need to be dried, allowing for the measurement of the mechanical properties of swollen hydrogels. Using this method we determine the Poisson's ratio of hydrogel particles composed of polyethylene glycol (PEG) and varying solvents fabricated using a lithography technique. The results demonstrate with high precision the dependence of the hydrogel compressibility on the solvent fraction and character. The method, easy to implement, can be adapted for the measurement of a variety of soft and biological materials.

## I. INTRODUCTION

Soft materials are found in situations as different as flow of biological fluids, biomedical devices, micro-fluidic sensors or soft micro-robotics for example in the form of soft polymeric particles or different types of protein or cell aggregates. Among soft materials, hydrogels are extremely powerful materials allowing particles of controlled shapes to be manufactured at the microscale. Their biocompatibility, their softness and their easy and rapid fabrication make them perfectly suited for biomedical applications like drug delivery [1, 2] or tissue engineering [3]. They are also useful as building blocks for the design of soft composite systems able to change shape in response to extrinsic stimuli, offering applications in soft robotics, in flexible electronics and development of biosensors [4]. Being able to precisely characterize their mechanical properties is essential when designing such applications, but faces specific problems, due to their small scale, the dependence of their properties on the surrounding or their ability to evolve over time.

The static linear mechanical properties of an isotropic elastic material are fully determined by two quantities: the Young's modulus ( $E$ ) and the Poisson's ratio ( $\nu$ ). In a compressive test the Young's modulus links stress and strain, whereas the Poisson's ratio quantifies the expansion of a material in directions perpendicular to the direction of compression. This Poisson's ratio varies, for an isotropic material, from 0.5 (incompressible) to -1. Other quantities such as the bulk modulus ( $K$ ), the shear modulus ( $G$ ) or the Lamé's first coefficient ( $\lambda$ ) correspond to different combinations of these two quantities [5].

Different techniques have been developed to measure the Poisson's ratio. The most straightforward method relies on the measurement of the strain in two orthogonal directions during a compressive test. Another method is to measure two different moduli, as the bulk modulus  $K$  and the Young's modulus  $E$ , and to obtain the Poisson's ratio using their relationship  $K = E/(3(1 - 2\nu))$ . Classical methods usually require a macroscopic sample, and

thus a significant volume of material which can be limiting for microscopic soft particles. Additionally, in these classical methods the sample often needs to be fixed onto the testing apparatus and thus requires the sample to be dried [6]. For the soft materials considered here, drying may have a strong impact on the microstructure and thus on the material properties. In addition, soft hydrogels may have internal timescales due to poroelasticity and/or viscoelastic effects, which may influence their mechanical responses depending on the frequency or time-scale of the chosen technique.

Some methods have been proposed to overcome these limitations, Wyss *et al.* [7] developed a simple method using microfluidics to measure the Poisson's ratio of a soft particle relying on the independent measurement of the bulk and the Young's modulus. However the experimental errors of each of these measurements, even more pronounced for soft materials, are limiting the accuracy of the determination of the Poisson's ratio only varying over a small range. Other techniques, such as micro-pipette aspiration experiments [8, 9] or atomic force microscopy (AFM) [10], provide high-accuracy measurements of the Poisson's ratio, but only probe locally the surface of the sample and do not provide bulk measurements. Acoustic waves can also be used to perform dynamic mechanical tests [11]. Usually the wave frequency varies from 0.5 to 5.0 MHz, and the measured elastic constants might be dependent on the frequency and differ from a static compression test. Finally, techniques such as small angle X-ray scattering [12] also enable the measurement of Poisson's ratio but require costly infrastructures.

In this article, we propose a simple and direct method to measure the Poisson's ratio of soft hydrogels at long times directly inside a microchannel. We use a microfluidic setup where hydrogel particles are fabricated and subsequently transported in a channel whose width is smaller than the particle width (see Figure 1). After the full entry of the particle into the narrow channel, the external flow is stopped and the particle is solely submitted to an uniaxial compression by the lateral walls. This ge-

ometry is well adapted to determine the Poisson's ratio by measuring at equilibrium the deformation of the particle in the direction of the uniaxial compression as well as in the perpendicular direction. This method being performed *in situ*, no drying step is necessary ensuring no modification of the structure of the material. Temporal observations of the hydrogel deformation allow for access to the inherent time dependence of the processes and to unequivocally determine the equilibrium state reached at long timescales. Due to poroelastic effects water can be squeezed out of the hydrogel under mechanical load, leading to the compressibility of the material. After detailing the method and its limitations we provide accurate measurements of Poisson's ratio of PEGDA hydrogels fabricated in different solvents.

## II. MATERIALS AND METHODS

### A. Channel and particle fabrication

PDMS (Polydimethylsiloxane, Sylgard 184, Corning) micro-channels are fabricated using traditional soft lithography techniques. The channels are bound to a coverslip covered with a thin layer of PDMS to have the same material on the four walls of the channel. The channels have a rectangular cross section and a constant height (either  $H = 57 \pm 3 \mu\text{m}$  or  $H = 103 \pm 3 \mu\text{m}$ ). They are composed of three regions: two linear channels with different width (a large channel in the order of mm and a small channel in the order of a few hundreds of micrometers) are connected by a constriction with a small angle (5 to 10 degrees).

Slabs of hydrogel with controlled geometry and position are directly fabricated inside the micro-channel using microscope-based photolithography [13]. This method has been extensively detailed in previous works [13–19], and just the essential steps are detailed here and schematically represented in Figure 1. The channel, filled with an oligomer solution and a photo-initiator, is exposed to a pulse of UV light of controlled duration. A mask with transparent drawings and black background is placed on the field-stop position of the microscope. The UV-light passes through the mask and forms its image in the focal plane of the microscope. Thus, only the part of the channel corresponding to the transparent part of the drawings is illuminated by the UV-light. Polymerization of the solution occurs in this region allowing for the fabrication of hydrogel particles whose geometry corresponds to the drawings on the mask. After fabrication, the particles are surrounded by the uncured solution. The position of the particle only depends on the position of the channel on the microscope, which can be adjusted by moving the stage. Because the method of fabrication is based on a 2D projection technique, the 3D geometry of the particle results from the polymerization of the PEGDA in the height of the channel. The permeability of PDMS to oxygen - which inhibits the cross-linking reaction - leaves a

non-polymerized lubrication layer of constant thickness on the top and bottom of the particles allowing particles to be freely transported in the channel.

In this work, we use an inverted microscope (Zeiss Axio Observer) equipped with a UV light source (Lamp HBO 130W) and a  $\times 5$  Fluar objective. The shutter (Uniblitz, V25), of 10 ms response time, is coupled with an external generator (Agilent 33220A) and allows for a very accurate control of the exposure time. We fabricate particles with a rectangular shape at zero flow rate in the wide region of the channel. The width  $w_0$  and length  $\ell_0$ , are determined by the dimensions of the drawings on the mask corrected with a factor that takes into account the objective magnification. The particle height is  $h_0 = H - 2b$  where  $H$  is the channel height, and  $b$  is the inhibition layer thickness (top and bottom), which we have been measured to be  $b = 6 \pm 1.6 \mu\text{m}$ . Due to the dimensions of the microchannel the height of the fabricated particle is always smaller than its width and length. The maximal dimensions of a particle are set by the UV-light beam diameter and is 1.5 mm in our setup. To ensure homogeneous crosslinking of the hydrogel we choose to limit the maximal dimensions of the particle to 1 mm.

The photosensitive solution is composed of an oligomer, polyethylenglycol diacrylate (PEGDA,  $M_n = 700 \text{ g/mol}$ , Sigma), a photoinitiator (PI, 2-hydroxy-2-methylpropiophenone, Sigma) and a solvent. The solvent can be either pure water or a mixture of water and polyethylenglycol (PEG<sub>1000</sub>,  $M_n = 1000 \text{ g/mol}$ , Sigma) in a proportion of 1:2. While the proportion of solvent varies, the proportion of photoinitiator is kept constant at 10%. The volume fraction of water varies from 0% to 50%. Above 50% the solution becomes biphasic and no particle can be fabricated. The maximal dilution with the PEG<sub>1000</sub>-water mixture is 70%. Table I shows the composition of the different solutions used in this study.

PEGDA	PI	water	PEG <sub>1000</sub> -water ratio 2:1 in volume	name
90%	10%	0%	0%	pure PEGDA
80%	10%	10%	0%	PW <sub>10</sub>
70%	10%	20%	0%	PW <sub>20</sub>
60%	10%	30%	0%	PW <sub>30</sub>
50%	10%	40%	0%	PW <sub>40</sub>
40%	10%	50%	0%	PW <sub>50</sub>
80%	10%	0%	10%	PP <sub>10</sub>
70%	10%	0%	20%	PP <sub>20</sub>
60%	10%	0%	30%	PP <sub>30</sub>
50%	10%	0%	40%	PP <sub>40</sub>
40%	10%	0%	50%	PP <sub>50</sub>
30%	10%	0%	60%	PP <sub>60</sub>
20%	10%	0%	70%	PP <sub>70</sub>

TABLE I. Volume fraction of each component of the different photosensitive solutions used in this study.

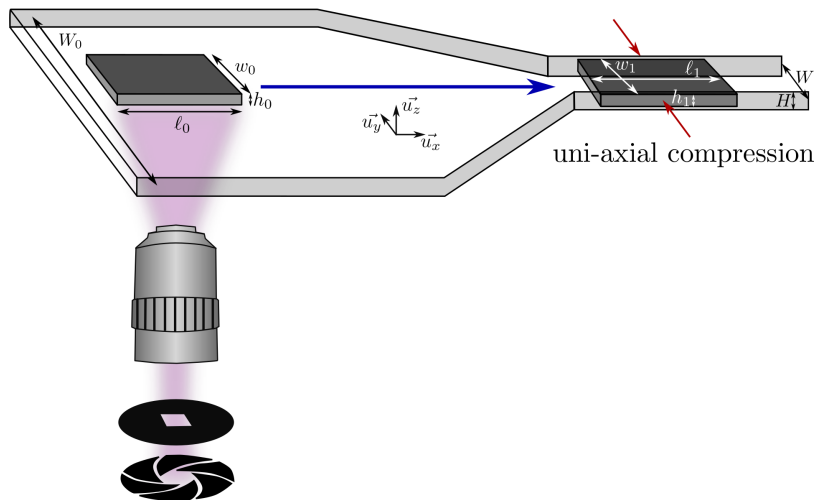


FIG. 1. (a) *In situ* fabrication of a particle using a microscope-based projection lithography technique. UV light is projected into a flat channel through a shutter and a rectangular mask resulting in the fabrication of a hydrogel particle surrounded by uncured solution. The slab is then pushed into a constriction by applying an external flow. When the particle has completely entered the narrow region of the channel the flow is stopped and the particle experiences uni-axial compression.

## B. Experimental protocol

The inlet of the micro-channel is connected to a reservoir, and a pressure controller (LineUP Series, Fluigent) is used to control the flow in the channel. Once the channel is filled with the photosensitive solution, the flow is stopped and a particle is fabricated. A picture of the particle is taken using a Hamamatsu Orca-flash 4.0 camera and gives a precise measure of the dimensions before deformation (see Figure 2 (a)). Then the particle is pushed through the constriction into the narrow channel by imposing a flow through a pressure difference along the channel varying from a few hundred mbars to 2 bars. Once the particle has entirely entered the narrow region the flow is turned off. There, the particle experiences uniaxial compression from the channel's lateral walls and we monitor its shape evolution with a frame rate of one image per second. Using standard image treatment procedures (with ImageJ [20] and MatLab) we extract the shape of the particle before and during deformation and measure the particle width, and length (see Figure 2 (c) and (d)). The length of the compressed particles decreases from its initial value to an equilibrium value (see Figure 2 (e)). In all our experiments we ensure to wait long enough ( $\sim 1200$ s) to measure the length  $\ell_1$  of the particle when this equilibrium is reached. At the end of the experiment, the particle is ejected from the narrow channel by imposing again a pressure driven flow. We repeat this procedure at least 10 times for each condition. In some cases, at the end of the experiment, the particle was transported back into the wide channel where the particle shape was measured after the flow had been stopped. We observed no residual deformation confirming the reversibility of the deformation and ruling out

any permanent deformations.

We vary the particle height ( $h_0 = 45 \pm 3 \mu\text{m}$  and  $h_0 = 91 \pm 3 \mu\text{m}$ ) and width ( $w_0 = 205 - 470 \mu\text{m}$ ) and the narrow channel width ( $W = 175 - 370 \mu\text{m}$ ). We keep the length of the particle constant and equal to  $\ell_0 = 960 \pm 8 \mu\text{m}$ . As can be seen in Figure 2 (b), the narrow channel is slightly deformed by the presence of the particle. We thus chose not to consider the width of the deformed particle to be equal to the width of the narrow channel but rather to measure  $w_1$  for each experiment. The particle width  $w_1$  differs only slightly from the channel width  $W$  and the importance of the difference between the two measures is given by the ratio of the Young's modulus of the PDMS ( $E_{PDMS} \sim 2 \text{ MPa}$ , [21]) and the hydrogel [18]. Particle deformation in the  $y$  direction will thus in the following be determined as  $w_0/w_1$  instead of  $w_0/W$ .

## C. Analysis

After the full entry of the particle into the narrow channel, the external flow is stopped and the particle is only submitted to an uniaxial compression by the lateral walls. We assume that the hydrogel is isotropic and homogeneous and linear elasticity thus gives:

$$\epsilon_{xx} = \frac{1}{E} [(1 + \nu)\sigma_{xx} - \nu(\sigma_{xx} + \sigma_{yy} + \sigma_{zz})] \quad (1)$$

$$\epsilon_{yy} = \frac{1}{E} [(1 + \nu)\sigma_{yy} - \nu(\sigma_{xx} + \sigma_{yy} + \sigma_{zz})] \quad (2)$$

$$\epsilon_{zz} = \frac{1}{E} [(1 + \nu)\sigma_{zz} - \nu(\sigma_{xx} + \sigma_{yy} + \sigma_{zz})] \quad (3)$$

with  $\sigma_{ii}$ ,  $\epsilon_{ii}$  respectively the compressive stress and

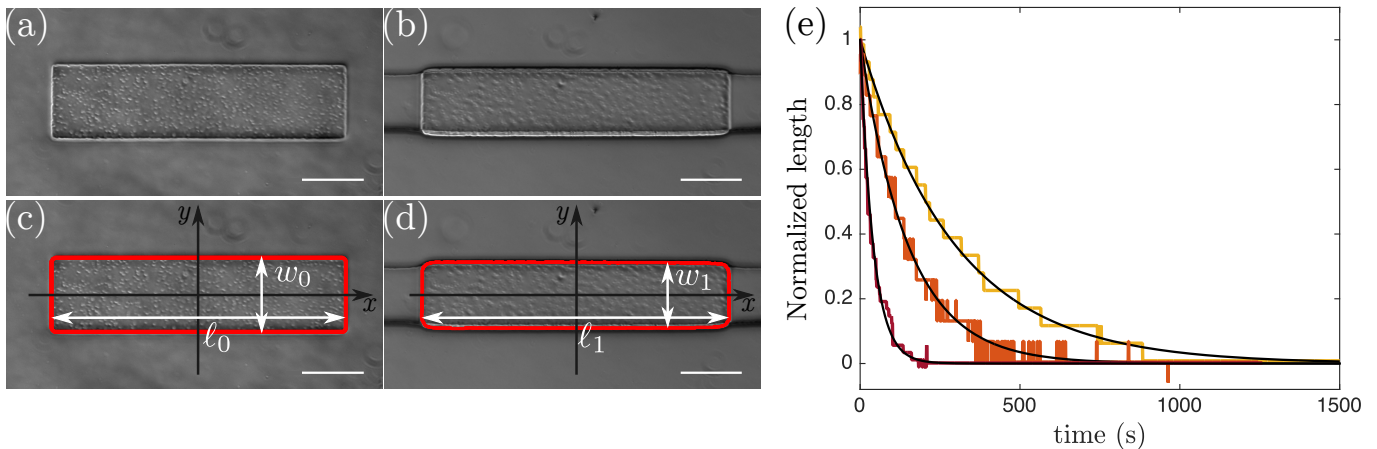


FIG. 2. Pictures of the slab in the wide (left column) and in the narrow (right column) channel. Top row corresponds to raw images of the undeformed (a) and deformed (b) particle. In (b) the dark region around the particle correspond to the channel walls. Bottom row shows the determination of the shape using ImageJ. Scale bars are 200  $\mu\text{m}$ . (e) Temporal evolution of the particle length after the flow has been stopped ( $t=0$ ). Length at time  $t$  is normalized by subtracting the equilibrium length and dividing by the difference between the initial length and the final length. Three different hydrogels are represented: from right to left, PP<sub>20</sub> (yellow), PP<sub>30</sub> (orange) and PP<sub>40</sub> (red). Exponential fits (black lines) are represented as a guide for the eyes.

strain in the particle.  $E$  is the Young's modulus of the hydrogel and  $\nu$  is its Poisson's ratio.

The particle being submitted to an uniaxial compression in the  $y$ -direction, one can write  $\sigma_{yy} = -P_{wall}$  and  $\sigma_{xx} = 0$ . Assuming that the deformed particle does not touch the top and bottom walls (*i.e.*  $h_1 < H$ ) there is no stress in the  $z$ -direction and  $\sigma_{zz} = 0$ . This last assumption has to be verified *a posteriori* by evaluating the strain in the  $z$ -direction.

Equations (1), (2) and (3) then become :

$$\epsilon_{xx} = -\frac{\nu}{E}\sigma_{yy}, \quad \epsilon_{yy} = \frac{1}{E}\sigma_{yy} \quad \text{and} \quad \epsilon_{zz} = -\frac{\nu}{E}\sigma_{yy} \quad (4)$$

#### D. Validation of the method

When the particle is compressed by the channel walls its length increases as can be seen on Figure 2 (a-d) and as expected for an elastic material. Figure 3 summarizes experiments where particles have been created in a PW<sub>30</sub> solution and compressed into a channel of constant width  $W = 175 \pm 0.7 \mu\text{m}$ . The initial particle width  $w_0$  is varied to apply varying confinements  $w_0/W$ . To extract the Poisson's ratio we compute the ratio  $\epsilon_{xx}/\epsilon_{yy}$  according to equations (4) taking into account that the width of the deformed particles is slightly different from the width  $W$  of the channel as a consequence of the deformation of the lateral channel walls (bottom of figure 3 (a)). Figure 3 (b) summarizes our measurements of  $\nu$  for different values of the confinement  $w_0/W$ . Each data point (blue circles) corresponds to one compressed particle and the average values and corresponding error bars are represented in black. Larger  $w_0/W$  induces stronger

deformation and thus larger stresses applied by the walls on the particle. On Figure 3 (b), the Poisson's ratio is independent of  $w_0/W$  in the range [1 1.53] corresponding to applied strain varying from  $-6.2\%$  to  $-17.7\%$ , validating our technique to measure a material property which is expected to be independent of the geometry, the applied stress and the resulting strain. For very small ratios  $w_0/W$  ( $w_0/W \leq 1.2$ , light gray region) particle deformation is small and large scatter of the data points is observed. For the widest particle ( $w_0 = 300 \mu\text{m}$ ), the stress is large enough to induce buckling (see image in Figures 4 (a) and (b)), leading to a saturation of  $l_1$  and preventing any measurement of the Poisson's ratio.

#### E. Limitations

Limitations are inherent to every technique and it is essential to take them into consideration when developing a new method. We discuss in the following section the range of validity for our microfluidic technique. First, our analysis relies on the assumption that the compressive stress is solely applied in the  $y$ -direction by the lateral walls of the narrow channel and thus the only stress component that is non-zero is  $\sigma_{yy}$ . For this to be true deformation in the vertical direction needs to be small enough so that the particle does not touch the channel top and bottom walls which would lead to an additional compressive stress  $\sigma_{zz}$  in the  $z$ -direction. This can be verified experimentally by comparing the height of the compressed particle to the channel height. The height of the deformed particle is  $h_1 = h_0 \exp(\epsilon_{zz}) \sim h_0(1 - \nu\epsilon_{yy})$  and the condition  $\sigma_{zz} = 0$  is verified as long as  $-h_0\nu\epsilon_{yy} < 2b$ . As a

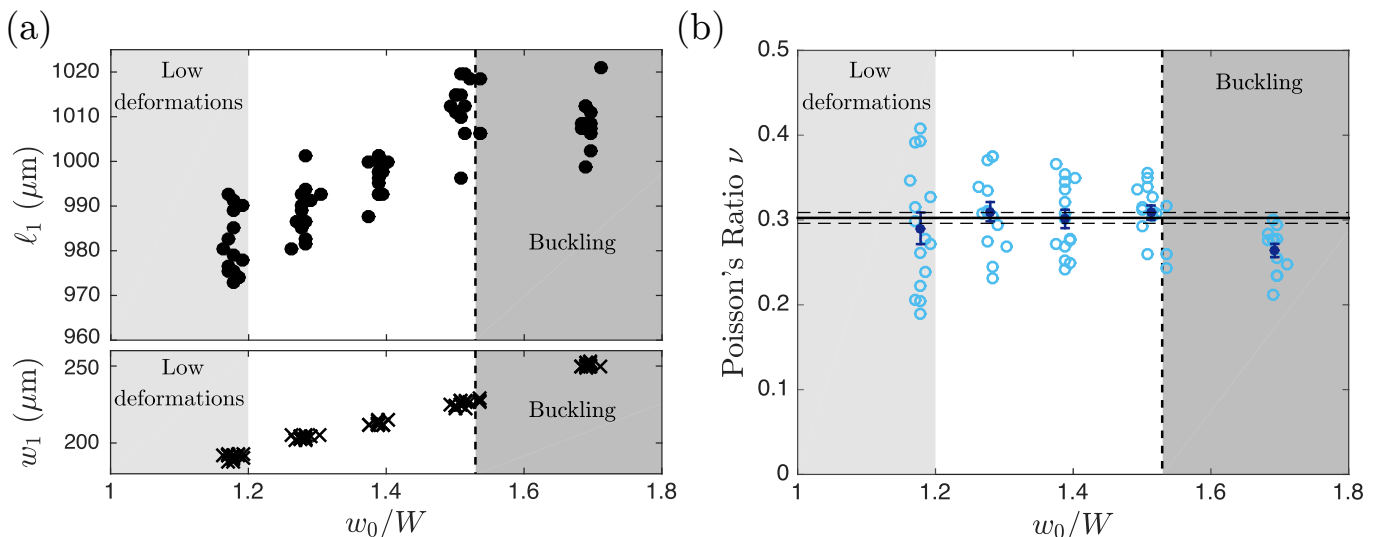


FIG. 3. Direct measurements of particle length and width and derivation of the Poisson's ratio. Results are shown for the hydrogel PW<sub>30</sub> in a channel of width  $W = 175 \pm 0.7 \mu\text{m}$  and height  $H = 103 \pm 3 \mu\text{m}$ . The initial particle length is kept constant  $l_0 = 960 \pm 8 \mu\text{m}$  while the confinement  $w_0/W$  is increased. (a) Length (top) and width (bottom) of the deformed particle at equilibrium as a function of the confinement  $w_0/W$ . (b) Evolution of the Poisson's ratio as a function of  $w_0/W$ . In (a) and (b) the light (dark) gray regions correspond to particle width that are too small (large) to ensure good precision of the determination of the Poisson's ratio. The vertical dotted line corresponds to the buckling threshold (see text). In (b) each light blue dot corresponds to a single experimental measurement, and dark blue markers correspond to their average and standard deviation  $\sigma$  normalized by  $\sqrt{n}$  with  $n = 15$  the number of independent measurements. Horizontal black lines correspond to the average (solid line) and standard deviation (dashed line) of all points except from the dark gray region ( $w_0/w_1 \geq 1.53$ ). The Poisson's ratio is found to be  $\nu_{30\%} = 0,302 \pm 0,007$  for the photosensitive solution PW<sub>30</sub>.

consequence the assumption is more likely to be verified for particles of small height  $h_0$  and for small deformations. In all our experiments we verify *a posteriori* that the deformed particle height remains smaller than the channel height and thus that the assumption  $\sigma_{zz} = 0$  is valid. We disregard experiments where this is not the case. Note also that the condition  $\sigma_{xx} = 0$  is not strictly verified close to the edges of the hydrogel particle due to the slight deformation of the PDMS channel (see Figure 2 (b) and (d)). This effect is more important for particles of large elastic modulus and strong compression  $\epsilon_{yy}$ , but is considered in all cases to be a small correction for our experiments.

Second, for too small confinements  $w_0/W$  particle deformation is small and the experimental accuracy of  $\nu$  is limited by the resolution of the deformed particle dimensions. The resolution can be improved either by applying stronger confinement (increasing the ratio  $w_0/W$ ) or by upscaling the experiment, increasing both  $w_0$  and  $W$ . We will see below that this can however favor buckling instabilities and is thus not in all cases a favorable option.

Third, when the slab is too wide buckling may occur preventing the Poisson's ratio to be measured. The critical stress to induce buckling of a thick elastic plate is given by  $\sigma_{yy}^{crit} = \alpha \pi^2 \frac{E}{12(1-\nu^2)} \left(\frac{h_0}{w_0}\right)^2$  [22, 23]. The correction factor  $\alpha$  depends on the ratio  $w_0/h_0$  and takes

into account the shear deformation in the height. According to [23]  $\alpha = 2.11$  for  $w_0/h_0 = 2$  and  $\alpha = 1.03$  for  $w_0/h_0 = 10$ . This critical stress is compared to the stress exerted by the lateral walls assuming linear deformation,  $\sigma_{yy} = \epsilon_{yy} E$ , via the dimensionless number

$$N = \frac{12(1-\nu^2)}{\alpha \pi^2} \left(\frac{w_0}{h_0}\right)^2 \epsilon_{yy} \quad (5)$$

If  $N > 1$  the particle buckles and, on the contrary, if  $N < 1$  the particle deforms linearly. The black vertical dotted line in Figure 3 corresponds to  $N = 1$  and good agreement between the theoretically predicted buckling threshold and the experimental observations is obtained. Buckling of the hydrogel particle is visible by direct observation (see Figures 4 (a) and (b)) but also from the saturation of  $l_1$  at strong confinement (see Figure 3 (a)) associated to the non-physical decrease of  $\nu$  seen on Figure 3 (b). Since the buckling threshold  $N$  depends on the Poisson's ratio as  $1 - \nu^2$ , variations of  $\nu$  between 0 and 0.5 induce only very small modifications of  $N$ . Thus the buckling threshold is mainly given by the geometry of the particle (via the particle aspect ratio  $w_0/h_0$ ) and the geometry of the channel (the strain  $\epsilon_{yy}$  being proportional to  $w_0/W$ ). In conclusion to avoid buckling, small  $\epsilon_{yy} \propto w_0/W$  and small aspect ratios ( $w_0/h_0$ ) are favorable.

To illustrate these findings, in Figure 4 (c) both the channel width and height have been modified compared

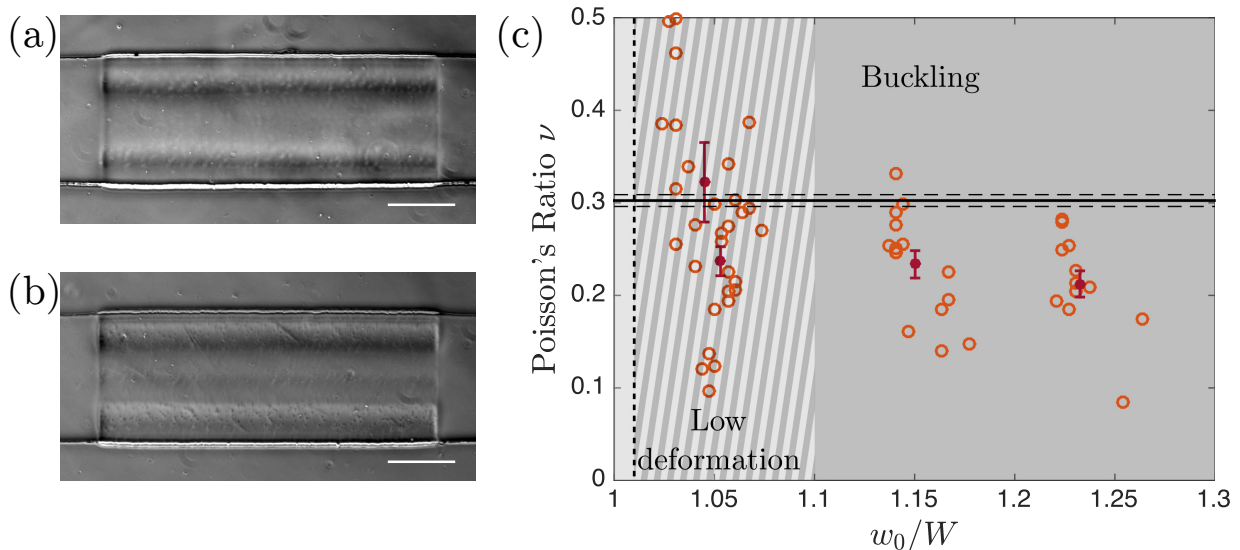


FIG. 4. Limitations of the method. Results correspond to experiments performed with hydrogel particles created with the  $PW_{30}$  photosensitive solution in a channel of width  $W = 370 \pm 1 \mu\text{m}$  and height  $H = 57 \pm 3 \mu\text{m}$ . (a) and (b) show two pictures of buckled particles, at least two wavelengths are visible in (a) and three in (b). They correspond respectively to  $w_0/W = 1.23$  and  $w_0/W = 1.36$ . (c) Evolution of the ratio  $-\epsilon_{xx}/\epsilon_{yy}$  as a function of  $w_0/W$ . Open circles represent the results of single experiments and dark red markers represent average values of the different experiments. The light/gray regions of Figure 3 (b) overlap for this example. Note that here also the measured ratio  $-\epsilon_{xx}/\epsilon_{yy}$  is lower than the Poisson's ratio when the particle buckles.

to Figure 3 while keeping the same photosensitive solution. The channel width  $W$  has been increased to have a better resolution and the limit of the light grey region is indeed pushed to a lower value of  $w_0/W$  ( $\approx 1.1$  to be compared to  $\approx 1.2$  in Figure 3 (b)). The channel width on the other side has been increased and the particles are thus more prone to buckle. The limit of the dark grey region is shifted to smaller values of  $w_0/W$  ( $\approx 1.01$  compared to  $\approx 1.53$  in Figure 3 (b)). As can be seen on the figure, despite the better resolution, the two grey regions overlap meaning that this channel geometry does not allow for Poisson's ratio measurements.

The comparison of the Figures 3 (b) and 4 (c) illustrates the compromise that has to be done between increasing the resolution on the particle deformation and avoiding particle buckling. A decrease of  $w_0$ , keeping  $h_0$  constant, increases the range of deformation before buckling but at the same time decreases the resolution. On the other hand, an increase of  $h_0$  alone is favorable to avoid buckling but should be limited to prevent the deformed particle to touch the top and bottom walls. While designing channels for such measurements, one has to keep these two opposite effects in mind and to choose the best geometry varying the channel width and height accordingly.

Finally, for very soft particle and thus weakly crosslinked hydrogel particles ( $PP_{60}$  and  $PP_{70}$  [18]), we observe a dependency of the equilibrium length ( $\ell_1$ ) on the velocity at which a particle enters into the constriction. A possible reason of this observation can be found

in the viscoelastic properties of the gel and/or the complex friction between the hydrogel and the lateral channel walls [24]. In such situations we consider that the measurement of the Poisson's ratio can not be achieved properly.

#### F. Dependence of the Poisson's ratio on the solvent composition

Using our method we measured the Poisson's ratio of hydrogels fabricated from different compositions of photosensitive solutions with different solvent concentrations and solvent nature. Figure 5 shows the measured Poisson's ratio for dilutions of PEGDA  $M_n = 700$  g/mol with water (blue points) and with a PEG<sub>1000</sub>-water mixture (2:1 in volume, purple points). In the absence of solvent the hydrogel is nearly incompressible ( $\nu_{0\%} = 0.50 \pm 0.01$ ) which is in agreement with the literature [25]. In presence of solvent, the hydrogel becomes compressible as shown by the decrease of the Poisson's ratio. This compressibility results from the flow of solvent molecules leaving the particle when the hydrogel is compressed and depends on the microstructure of the cross-linked polymeric chains of PEGDA. Note that during an isotropic compression as would be imposed by a static pressure the hydrogel particles are incompressible, as a consequence of the incompressibility of water. For larger dilution of the photosensitive solution, the fraction of solvent increases leading to a smaller Poisson's ratio. In addition, we observe that for the same dilution, the Poisson's ratio is always smaller

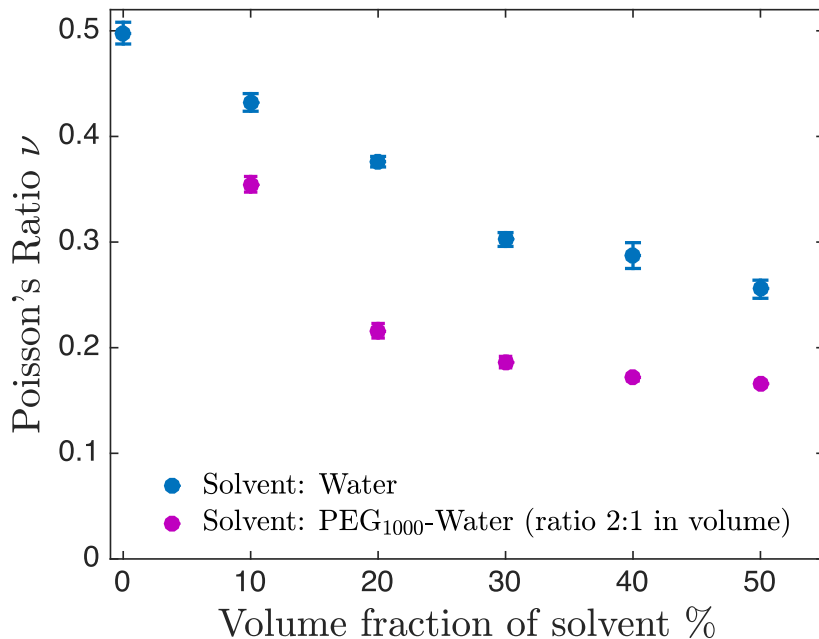


FIG. 5. Evolution of the Poisson's ratio of hydrogels fabricated from different photo-sensitive solutions as a function of the solvent volume fraction. Two different solvents are shown: water (blue markers) and a solution of PEG  $M_n = 1000$  g/mol -water at a ration 2:1 in volume (purple markers).

in PEG<sub>1000</sub>-water compared to pure water: In water, the lowest value measured is  $\nu_{50\%} = 0.255 \pm 0.009$  while in PEG<sub>1000</sub>-water this value is  $\nu_{50\%} = 0.165 \pm 0.002$ . The decreased value of the Poisson's ratio reported here is a signature of the modified microstructure of the hydrogels. Further work is however necessary to fully understand the impact of the presence of chains of PEG in the surrounding medium on the compressibility of the hydrogels. Several hypothesis can be however be proposed: first, the presence of PEG is known to increase the porosity of the hydrogel [26] which is expected to modify the mechanical properties. The presence of PEG chains probably also impacts the connectivity of the meshwork as well as the chemical potentials of the different species.

The flow of solvent through the polymeric mesh will induce poroelastic effects, explaining the temporal evolution of the particle length shown in Figure 2 (e). Poroelasticity indeed describes the flow of solvent through the mesh of a deformable material and introduces a time-dependent response to deformation. According to references [27] and [28] this poroelastic phenomenon is expected to depend on the porosity of the hydrogel and the viscosity of the solvent. The three different photo-sensitive solutions used in Figure 2 (e), PP<sub>20</sub> (yellow), PP<sub>30</sub> (orange) and PP<sub>40</sub> (red), have comparable viscosities ( $\mu^{PP_{20}} = 108 \pm 3$  mPa·s,  $\mu^{PP_{30}} = 107 \pm 3$  mPa·s and  $\mu^{PP_{40}} = 116 \pm 3$  mPa·s). On the contrary, the mesh size decreases with increasing dilution as the polymer chains are further apart during crosslinking in the presence of solvent molecules. This is in good agreement with the tendency shown in Figure 2 (e) in which the characteristic poroelastic time decreases when the

solvent fraction increases. Note that as the poroelastic timescale also depends on the dimensions of the hydrogel, the timescales for micron-scale particles as in the present study are much smaller than for macroscopic particles [27, 28]. Let us state again here that all our measurements have been performed at equilibrium to prevent any impact of these temporal effects on our measurement of the hydrogel compressibility.

### III. CONCLUSION

Until now we have considered homogeneous materials and shown that our experimental technique is well-suited to determine the Poisson's ratio of the material they are made of. Figure 6 shows the extension of our technique to metamaterials in which the geometry of the structure changes the mechanical properties. In this example, an auxetic particle has been fabricated using a specific design of the structure [29]. The superposition of the shapes of this particle before (gray) and after (black) introduction into the narrow channel clearly shows that the particle is slightly shorter when compressed which is the signature of a negative Poisson's ratio.

We have presented a new technique for the measurement of the Poisson's ratio of micrometric soft hydrogels with a very good measurement accuracy. The absolute measurement errors varying from 0.002 to 0.012 are comparable to what is obtain using X-ray diffraction [12], and are much smaller than for measurements relying on the determination of two independent elastic moduli [7, 30]. We successfully used this approach to measure Poisson's

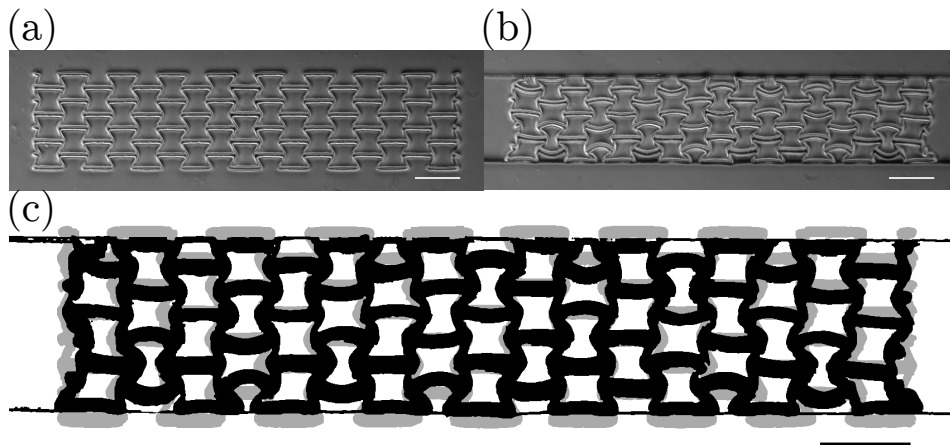


FIG. 6. Auxetic metamaterial fabricated from a solution of 90% of PEG-DA  $M_n = 700$  g/mol and 10% of photo-initiator in volume. (a) Before compression, (b) submitted to an uniaxial compression, (c) superposition of the undeformed and deformed shape. The particle width as well as its length decrease while compressed, signature of a negative Poisson's ratio.

ratio of different hydrogels and show that this Poisson's ratio varies on a large range of values (0.165 to 0.5). We discussed the limitations of the methods and shown how channel and particle geometries should be chosen to accurately measure the Poisson's ratio. Compared to other approaches an important advantage of our method is that it is done *in situ* directly in the surrounding fluid and does not require any drying of the sample. Another advantage as compared to atomic force microscopy (AFM) which probes the mechanical properties at nanometer scale is the determination of the mechanical property - the Poisson's ratio in our case - of the entire hydrogel particle on a scale much larger than the pore sizes even for very porous materials. Moreover, the technique presented here, allows for an excellent measurement of the dynamical response of the material enabling the determination of the Poisson's ratio at long times and thus at equilibrium. Our characterization method is not limited to particles directly fabricated inside a microchannel but can also be used for example for protein or cell aggregates that can be flown into the microchannel. However their potentially more complex shape and porosity can make the

analysis less straight forward [31] and would require the use of effective strains and stresses to describe the particle deformation [32]. Moreover, if the condition  $\sigma_{zz} = 0$  is not verified, our method could be adapted to measure the Poisson's ratio, that in that case, derives from the formula  $\nu/(1 - \nu) = -\epsilon_{xx}/(\epsilon_{yy} + \epsilon_{zz})$ . Because of these advantages and its simplicity we think this method will be used for the characterization of the Poisson's ratio of many different soft objects from nature or industry.

#### ACKNOWLEDGMENTS

We thank Al Crosby for inspiring discussions and Charles Duchne for help with the experimental set-up.

This research was funded by the European Research Council through a consolidator grant (ERC PaDyFlow 682367). This work received the support of Institut Pierre-Gilles de Gennes (Équipement d'Excellence, "Investissements d'Avenir", Program ANR-10-EQPX-34).

- 
- [1] S. Nayak, H. Lee, J. Chmielewski, and L. A. Lyon, "Folate-mediated cell targeting and cytotoxicity using thermoresponsive microgels," *Journal of the American Chemical Society*, vol. 126, no. 33, pp. 10258–10259, 2004.
  - [2] K. S. Soppimath, D.-W. Tan, and Y.-Y. Yang, "ph-triggered thermally responsive polymer core-shell nanoparticles for drug delivery," *Advanced materials*, vol. 17, no. 3, pp. 318–323, 2005.
  - [3] L. Ambrosio, R. De Santis, and L. Nicolais, "Composite hydrogels for implants," *Proceedings of the Institution of Mechanical Engineers, Part H: Journal of Engineering in Medicine*, vol. 212, no. 2, pp. 93–99, 1998.
  - [4] Y. Liu, J. Genzer, and M. D. Dickey, "?2d or not 2d?: Shape-programming polymer sheets," *Progress in Polymer Science*, vol. 52, pp. 79–106, 2016.
  - [5] S. H. Crandall, T. J. Lardner, R. R. Archer, N. H. Cook, and N. C. Dahl, "An introduction to the mechanics of solids," 1978.
  - [6] Y. Li, Z. Hu, and C. Li, "New method for measuring poisson's ratio in polymer gels," *Journal of applied polymer science*, vol. 50, no. 6, pp. 1107–1111, 1993.
  - [7] H. M. Wyss, T. Franke, E. Mele, and D. A. Weitz, "Capillary micromechanics: Measuring the elasticity of microscopic soft objects," *Soft Matter*, vol. 6, no. 18, pp. 4550–4555, 2010.

- [8] J. Li, *Advances in Chemical Engineering: Characterization of Flow, Particles and Interfaces*, vol. 37. Academic Press, 2009.
- [9] T. Boudou, J. Ohayon, C. Picart, and P. Tracqui, “An extended relationship for the characterization of young’s modulus and poisson’s ratio of tunable polyacrylamide gels,” *Biorheology*, vol. 43, no. 6, pp. 721–728, 2006.
- [10] D. C. Hurley and J. A. Turner, “Measurement of poisson’s ratio with contact-resonance atomic force microscopy,” *Journal of Applied Physics*, vol. 102, no. 3, p. 033509, 2007.
- [11] K. Evans, *Measurement of Poisson’s Ratio*. Springer, 1999.
- [12] M. Moram, Z. Barber, and C. Humphreys, “Accurate experimental determination of the poisson’s ratio of gan using high-resolution x-ray diffraction,” *Journal of applied physics*, vol. 102, no. 2, p. 023505, 2007.
- [13] D. Dendukuri, P. Panda, R. Haghgoie, J. M. Kim, T. A. Hatton, and P. S. Doyle, “Modeling of oxygen-inhibited free radical photopolymerization in a PDMS microfluidic device,” *Macromolecules*, vol. 41, no. 22, pp. 8547–8556, 2008.
- [14] J. S. Wexler, P. H. Trinh, H. Berthet, N. Quennou, O. du Roure, H. E. Huppert, A. Linder, and H. A. Stone, “Bending of elastic fibres in viscous flows: the influence of confinement,” *Journal of Fluid Mechanics*, vol. 720, pp. 517–544, 2013.
- [15] H. Berthet, O. du Roure, and A. Lindner, “Microfluidic Fabrication Solutions for Tailor-Designed Fiber Suspensions,” *Applied Sciences*, vol. 6, no. 12, p. 385, 2016.
- [16] C. Duprat, H. Berthet, J. S. Wexler, O. du Roure, and A. Lindner, “Microfluidic in situ mechanical testing of photopolymerized gels,” *Lab on a chip*, vol. 15, no. 1, pp. 244–52, 2014.
- [17] M. Nagel, P.-T. Brun, H. Berthet, A. Lindner, F. Gallaire, and C. Duprat, “Oscillations of confined fibres transported in microchannels,” *Journal of Fluid Mechanics*, vol. 835, pp. 444–470, 2018.
- [18] J. Cappello, M. Bechert, C. Duprat, O. du Roure, F. Gallaire, and A. Lindner, “Transport of flexible fibers in confined microchannels,” *Physical Review Fluids*, vol. 4, no. 3, p. 034202, 2019.
- [19] M. Bechert, J. Cappello, M. Daïeff, F. Gallaire, A. Lindner, and C. Duprat, “Controlling transport dynamics of confined asymmetric fibers,” *arXiv preprint arXiv:1903.00761*, 2019.
- [20] C. A. Schneider, W. S. Rasband, and K. W. Eliceiri, “HISTORICAL commentary NIH Image to ImageJ : 25 years of image analysis,” *Nature Methods*, vol. 9, no. 7, pp. 671–675, 2012.
- [21] T. Gervais, J. El-Ali, A. Günther, and K. F. Jensen, “Flow-induced deformation of shallow microfluidic channels,” *Lab on a Chip*, vol. 6, no. 4, pp. 500–507, 2006.
- [22] R. M. Jones, *Buckling of bars, plates, and shells*. Bull Ridge Corporation, 2006.
- [23] M. E. Onyia and E. O. Rowland-Lato, “Determination of the Critical Buckling Load of Shear Deformable Unified Beam,” *International Journal of Engineering and Technology*, vol. 10, no. 3, pp. 647–657, 2018.
- [24] J. P. Gong, “Friction and lubrication of hydrogels?its richness and complexity,” *Soft matter*, vol. 2, no. 7, pp. 544–552, 2006.
- [25] S. Gabler, J. Stampfl, T. Koch, S. Seidler, G. Schuller, H. Redl, V. Juras, S. Trattng, and R. Weidisch, “Determination of the viscoelastic properties of hydrogels based on polyethylene glycol diacrylate (peg-da) and human articular cartilage,” *International Journal of Materials Engineering Innovation*, vol. 1, no. 1, pp. 3–20, 2009.
- [26] A. G. Lee, C. P. Arena, D. J. Beebe, and S. P. Palecek, “Development of macroporous poly (ethylene glycol) hydrogel arrays within microfluidic channels,” *Biomacromolecules*, vol. 11, no. 12, pp. 3316–3324, 2010.
- [27] S. Cai, Y. Hu, X. Zhao, and Z. Suo, “Poroelasticity of a covalently crosslinked alginate hydrogel under compression,” *Journal of Applied Physics*, vol. 108, no. 11, p. 113514, 2010.
- [28] Y. Hu, X. Zhao, J. J. Vlassak, and Z. Suo, “Using indentation to characterize the poroelasticity of gels,” *Applied Physics Letters*, vol. 96, no. 12, p. 121904, 2010.
- [29] X. Ren, R. Das, P. Tran, T. D. Ngo, and Y. M. Xie, “Auxetic metamaterials and structures: A review,” *Smart materials and structures*, vol. 27, no. 2, p. 023001, 2018.
- [30] M. T. Punter, B. E. Vos, B. M. Mulder, and G. H. Koenderink, “Poroelasticity of (bio) polymer networks during compression: theory and experiment,” *Soft Matter*, 2020.
- [31] C. Duchêne, V. Filipe, S. Huille, and A. Lindner, “Clogging of microfluidic constrictions by monoclonal antibody aggregates: role of aggregate shape and deformability,” *Soft Matter*, vol. 16, no. 4, pp. 921–928, 2020.
- [32] Y. Bommireddy, A. Agarwal, V. Yettella, V. Tomar, and M. Gonzalez, “Loading-unloading contact law for microcrystalline cellulose particles under large deformations,” *Mechanics Research Communications*, vol. 99, pp. 22–31, 2019.